TUNDRA FIRE DRIVEN SURFACE SUBSIDENCE INCREASES SPECTRAL DIVERSITY ON THE YUKON-KUSKOKWIM DELTA, ALASKA

BY

DUNCAN ANDERSON

THESIS

Submitted in partial fulfillment of the requirements
for the degree of Master of Science in Geography
in the Graduate College of the
University of Illinois Urbana-Champaign, 2023

Urbana, Illinois

Advisors:

Assistant Professor Mark J. Lara
Adjunct Assistant Professor Piotr Cienciala

ABSTRACT

Tundra fires can dramatically influence plant species cover and abundance, organic layer depth, and the magnitude of seasonal permafrost thaw. However, the potential impact of wildfire on short and long-term interactions between vegetation and permafrost thaw remains poorly understood. We evaluated the spatial and temporal interactions between wildfire and surface subsidence on a remotely derived proxy for species diversity (i.e., spectral diversity). Spectral diversity and rates of surface subsistence were calculated using airborne hyperspectral AVIRIS-NG imagery and spaceborne interferometric synthetic aperture radar (InSAR) data from Sentinel-1. Spectral diversity was measured as the spectral variance within a plant community (alpha-diversity), between plant communities (beta-diversity), and across terrain composed of a mosaic of communities (gamma-diversity). The Yukon-Kuskokwim Delta in southwestern Alaska is one of the warmest and most productive tundra regions, with a documented history of upland fires, 16 of which were examined within the Izaviknek and Kingaglia uplands which occurred between 1971 and 2015. Results indicate the burn scars had consistently lower total gamma diversity and higher rates of subsidence than paired unburned reference areas, where both gamma diversity ($R^2 = 0.74$, $p < 0.001$) and subsidence ($R^2 = 0.75$, $p < 0.001$) decreased with the time since burn. Where, younger burn scars had both a higher gamma diversity (0.013) and subsidence rates (-0.097 cm day^{-1}) than old scars with 0.005 and -0.053 cm day^{-1}, respectively. Gamma diversity was also found to have a negative relationship with subsidence rates ($R^2 = 0.63$, $p < 0.001$) where communities subsiding at a higher rate were more diverse. This study suggests that the patterns of plant species diversity and succession following wildfires are amplified by the thickening of active layers and surface subsidence that results in increased spectral diversity over 15 years following fire. These findings highlight the short and long-term

ecological interactions that impact post-fire spectral-species succession that influence tundra ecosystem structure and function.

ACKNOWLEDGMENTS

I have deep appreciation to all those who have supported me through my master's journey. Thanks to Dr. Mark Lara for his continual optimism, support, mentorship, and understanding. Thanks to Dr. Piotr Cienciala for his advice, support, and mentorship through shifting research and positions, and guidance out in the field. Thanks to Dr. Roger Michaelides from the Department of Earth, Environmental, and Planetary Sciences at the University of Washington in St. Louis for his expertise with synthetic aperture radar and service on my committee in helping to improve this work. Thanks to all of my lab mates, including our favorite lab pup Copper, and peers in the Geography and GIS department who have provided support, feedback, and friendship along this journey. Thanks to Emma Hall for welcoming me to her hometown and making me feel at home in my first year, far from North Carolina. Thanks to all my peers, friends, and faculty in the Geography and GIScience department and around Champaign-Urbana who have provided help, advice, and a resilient support system during these years. Thanks to Evan Stoor for his companionship, affection, and support which has made my last semester an invigorating adventure. Lastly, thanks to my family for their everlasting support and understanding in this endeavor and all those I will embark on in the future.

This research was supported by a seed grant from the Taylor Geospatial Institute, NASA-ABoVE (80NSSC22K1254), and NSF-EnvE (1928048).

In memory of my grandpa Fred, who helped instill in me a love of science from an early age, and my grandparents Lee and Jean.

TABLE OF CONTENTS

CHAPTER 1: INTRODUCTION

Tundra ecosystems are warming four times faster than the global average (Jacobs et al., 2021). As warmer and drier conditions increase the prevalence of wildfire activity (Hu et al., 2015), rates of permafrost thaw and overall vegetation change may increase (Michaelides et al., 2019; Mackay, 1995; Rocha et al., 2012; Jones et al., 2015). These interactions have been observed in the Yukon-Kuskokwim Delta as tundra fires were shown to alter spatial and temporal patterns of permafrost thaw and coincident recolonization of shrubs (Frost et al., 2020; Michaelides et al., 2019; Sae-Lim et al., 2019; AICC, 2023). Specifically, both deciduous and evergreen shrubs and bryophytes were found to colonize burn scars while lichen cover was found to be greatly diminished in recent burn scars and only significantly recovered in scars 45 years old or greater (Frost et al., 2020). Despite observations suggesting potential linkages between fire, vegetation, and permafrost thaw, knowledge of how these factors combine to affect the recovery of key ecosystem properties (i.e., biodiversity, productivity, permafrost) remains limited, yet important for understanding the potential consequences of the present and projected intensity and severity of tundra fires (French et al., 2015; Pastick et al., 2017).

Spectral diversity has emerged as a useful remote sensing proxy of plant species diversity, which is computed as the variability of reflected electromagnetic radiation from plant functional types and plant species, where the collection of pixels with greater spectral variance is often more diverse (Rocchini et al., 2010; Wang and Gamon, 2019). A variety of approaches have been developed to estimate spectral diversity using the spectra from aerial hyperspectral imagery, satellite multispectral imagery, using new indices such as Rao's Q, established indices such as measuring difference in NDVI, and directly measuring and quantifying variance in spectral bands (Wang and Gamon, 2019; Rossi et al., 2021). Few approaches have been able to

disaggregate spectral diversity into plant community metrics capable of simultaneously estimating alpha-diversity (i.e., diversity within a plant community), beta-diversity (i.e., diversity differences between plant communities), and gamma-diversity (i.e., landscape-level diversity), useful for evaluating the impact of regional-scale environmental change and disturbance processes on local-scale diversity (e.g., Whittaker, 1972). Laliberté et al (2020) recently developed methods to quantify these spectral diversity metrics from measuring spectral variance from hyperspectral imagery, though did not define communities used for the analysis by species or plant functional type composition. The use of hyperspectral imagery presents a further evolution of spectral diversity applications that have previously relied on larger landscape scale estimations of beta diversity from coarse multispectral satellite imagery. Nelson et al. (2022) conducted a dimensionality analysis revealing that in tundra ecosystems spectral diversity was variable across small scales (<10 km) and found that hyperspectral imagery presented a large advantage over multiband sensors in detecting spectral diversity in the studied ecosystem.

Spectral diversity applications have included broad mapping of diversity using multispectral satellites (Perrone et al., 2023; Rossi and Gholizadeh, 2023) and high-resolution aerial mapping of plot-scale communities, typically with hyperspectral imagery (Féret and Asner 2014; Gholizadeh et al., 2019; Van Cleemput et al., 2023), however there has been relatively few applications within boreal-arctic landscapes, though increased knowledge of spectral diversity applications is being built on lower latitude grasslands and forests relative to the boreal-arctic (Wang and Gamon, 2019; Kacic and Kuenzer, 2022). Prior applications which used hyperspectral imagery were collected with a wide variety of sensors, some being private, with few applications using widely available imagery products, for example the Airborne Visible InfraRed Imaging Spectrometer (AVIRIS) platform which has been used to measure spectral

diversity with both Classic and Next Generation (NG) sensors. AVIRIS Classic has been used to measure spectral diversity between managed agriculture and a mixture of unmanaged forest, shrub, and herbaceous cover in western Michigan, USA to identify diversity variability between managed agriculture and unmanaged land cover (Dahlin, 2016). In Hawai'i, AVIRIS Classic was used to evaluate biodiversity trends via spectral diversity in rainforests which correlated with field data (Carlson et al., 2007). In India, AVIRIS-NG imagery was used by Jha et al. (2019) to characterize species and forest health using a map of alpha spectral diversity and by Chaurasia et al. (2020) to examine biodiversity across different climactic sites in western Indian forests. Using a different hyperspectral sensor, McPartland (2019) examined species and spectral diversity of tundra and boreal vegetation under warming and conditions and hydrologic change within peatlands at the Alaska Peatland Experiment (APEX) near Fairbanks, AK, USA and within boreal forests at the Spruce and Peatland Responses Under Changing Environments (SPRUCE) experiment in northern Minnesota, USA. Comparisons of aerial hyperspectral imagery, plot-scale canopy spectra and vegetation cover samples found success in correlating spectral diversity with species diversity in both ecosystems. The AVIRIS-NG platform has a growing catalog of flights in Alaskan arctic-boreal ecosystems which spectral diversity methods can use to investigate diversity responses to disturbance including permafrost degradation and wildfire activity that affect ecosystem function.

Here we expand upon previous spectral diversity methodologies for investigating the coincident impact of historical tundra fires and surface subsidence on alpha, beta, and gamma diversity on the Yukon-Kuskokwim River Delta in southwestern Alaska. To advance our understanding of interacting disturbance regimes, we compute alpha, beta, and gamma spectral diversity using AVIRIS-NG and compare spectral metrics (1) among newly synthesized plant

community boundaries derived from hierarchical clustering of existing plant functional type (PFT) maps, (2) within a chronosequence of fire scars between 1971 and 2015, and (3) with Interferometric Synthetic Aperture Radar (InSAR) derived decadal surface subsidence trends and existing InSAR-derived soil moisture and active layer thickness (Chen et al., 2022). Results provide new methodologies and knowledge of decadal patterns of post-fire vegetation responses to coincident patterns of surface subsidence and environmental change (e.g., active layer thickness and soil moisture).

CHAPTER 2: SITE DESCRIPTION AND METHODS

2.1. SITE DESCRIPTION AND FIRE HISTORY

The Yukon-Kuskokwim Delta (YKD) is the largest river delta in western North America, with importance to coastal migratory bird populations, and contains a large indigenous population (Gill and Handel, 1990; Jorgenson et al., 2018; Rearden and Fienup-Riordan, 2014). The YKD has a well-documented fire history from modern monitoring programs (AICC, 2023) and historic reconstructions from charcoal records (Chipman et al., 2015) and is projected to experience continued permafrost degradation in part from increased wildfire activity (Pastick et al., 2015). Fire activity in the broader ecoregion has been episodic, with 8-14 years between seasons of higher fire activity and with recorded burns since 1953 totaling 5,818 km^2 (Rocha et al., 2012; AICC 2023; Nowacki et al., 2001). This study focuses on one of the relatively active areas, the Izaviknek and Kingaglia uplands (IKU), located ~74 km northwest of Bethel (figure 1). Annual maximum and minimum temperatures in July and January are 13.1 ℃ and -15.0 ℃, respectively (SNAP, 2022). Long-term precipitation normals from Bethel indicate the region experiences ~419 mm of annual precipitation, with monthly totals peaking in August at 83 mm (ACRC, 2023). Growing season length for this site typically starts on April 23rd and ends on October 27th, as we estimated from MODIS snow cover estimates between 2000-2022, following Hall et al. (2016).

Fifteen wildfires occurred within the area imaged by AVIRIS-NG in our study region on the IKU between 1971 to 2015 (table 1). The 2015 fire season was particularly active with 87,573 acres burned, almost double the area burned from all other years. Monitoring Trends in Burn Severity (MTBS) (only available for Aropuk, Kuka, Izavlknek River, and Kuka Creek 4) identified DNBR(x1000) values ranging from 229 to 368 with all fires being thematically

classified as of moderate severity (2023). Fire boundaries acquired from the Alaska Interagency Coordination Center (AICC) via the Alaska Forest Service were modified to address overlapping burn scars within the documented range and fires that occurred after AVIRIS-NG data collection. (figure 1). Repeatedly burned terrain between 1971 and 2015 were removed from our dataset and not considered in further analysis to minimize any potential artifacts or inconsistencies in our spectral or subsidence products that we were unable to constrain due to limited observations. Further, we created unburned reference areas using 1 km buffers around all burn scars, where overlapping burn and unburned buffer areas were removed (figure 1).

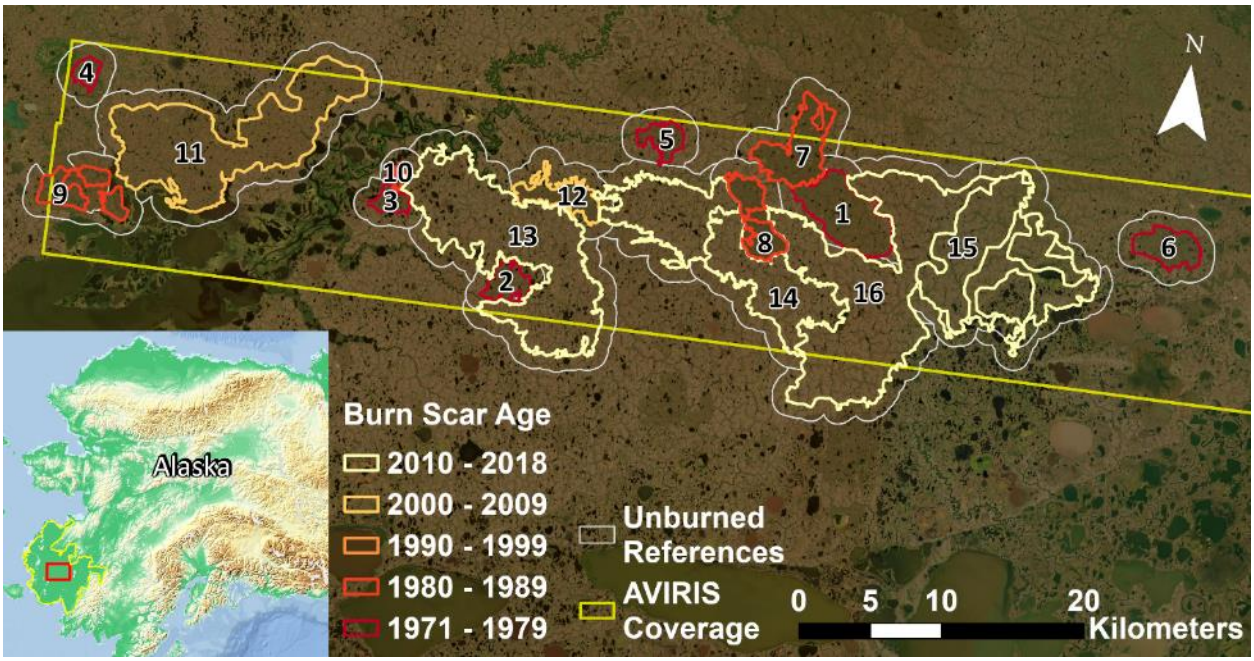

Figure 1. Map of selected known fires in the Izaviknek-Kingaglia uplands of the Yukon-Kuskokwim Delta from 1971 - 2015 with AVIRIS-NG flightline coverage. Fire perimeters adapted from the Alaska Fire Service, edited to remove overlapping burns. Unburned reference areas created from manually adjusted 1 km buffers shown.

Table 1. Summary of fire characteristics including estimated monitoring trends in burn severity (MTBS) mean severity where available.

Map No.	Name	Burn Year	Fire Out Date	Square Km Burned
1	Water	1971	7/7/1971	23.3
2	Smitty	1972	n/a	6.4
3	Dry Gulch	1972	n/a	3.7
4	Hobbs Knobb	1972	n/a	3
5	POM	1972	n/a	5.5
6	Long Lake	1972	7/11/1972	9.8
7	Yukon Delta NWR 2	1985	9/1/1985	17.8
8	Kasigluk	1985	8/14/1985	12.6
9	Tik Hill	1987	6/19/1985	14.5
10	DOF No. 8014014	1988	7/2/1988	1.3
11	Aropuk	2002	7/21/2002	81.8
12	Kuka	2007	8/9/2007	9.7
13	Izavlknek River	2015	8/26/2015	91.5
14	Kuka Creek 1	2015	7/7/2015	38.1
15	Kuka Creek 3	2015	6/30/2015	56.4
16	Kuka Creek 4	2015	8/6/2015	168.4

2.2 MAPPING OF PLANT COMMUNITIES

To calculate and partition spectral diversity, a spatial definition of community is required. Previous work has used a community delineation in the sense of a "sampling unit" where imagery is split into gridded near-uniform square plots of a given size, in the aforementioned application, a 20 m x 20 m grid was used (Wang and Gamon, 2019). While artificial, this unit was chosen as it corresponds to sampling plots that ecologists broadly use and is appropriate for situations where there is not *a priori* knowledge of the community composition of the entire spectral product, producing dozens or more communities depending on the resolution and spatial extent of the imagery as well as the selected plot size. Therefore, we defined plant communities using existing PFT fractional cover maps for use in subsequent spectral diversity calculations. Macander et al. (2022) derived a 30 m spatial resolution PFT maps (i.e., lichen, graminoid) on 5-

year intervals for the state of Alaska using visual and quantitative vegetation cover estimates from the ground, helicopters, planes, and unmanned aerial systems. Because of high fire activity in 2015 on the IKU, and the collection of five AVIRIS-NG flights occurring in 2018 (table 2), we only used the 2020 PFT map in subsequent community definitions.

Similar to traditional plant community definitions using plot-level species cover and abundance data, a hierarchical clustering analysis was used to determine community classifications from the mapped fractional cover with a variety of linkage methods tested to compare agglomerative coefficients (McCune and Grace, 2002). Prior to clustering, the fractional PFT cover layers were masked to remove (1) pixels sourced from years prior to or including 2015 when major fires occurred, (2) pixels outside our selected fires and corresponding unburned areas, and (3) pixels that had 0% cover in all PFTs, representing standing water or bare ground. To perform the clustering 15,000 pixels were randomly selected from the seven PFT map layers within the combined burn scars and unburned area from the PFT maps. The fractional cover of each functional type passed a Kolmogorov-Smirnov similarity test at the 0.05 level indicating the sample was representative of the whole PFT dataset.

This sample was clustered with five linkage methods (average, complete, single, Ward's, and weighted average) using the *agnes* function of the *cluster* R package (Maechler et al., 2022) and their agglomerative coefficients were compared to determine the best method, with Ward's distance method being the most successful (table 2). Ward's distance method was implemented following Ward's Criterion to cluster communities (McCune and Grace, 2002; Murtagh and Legendre, 2014). To identify how many clusters should be generated, the gap statistic K was generated for cluster numbers 1 to 25, and breaks were considered at points where diminishing returns on K from increasing the number of clusters was observed (see figure 4 in section 3.1).

Nine clusters were selected to best represent *in situ* plant community definitions, similar to that described in Frost et al. (2020). The clustered samples were used as an input to a random forest classifier, where 70% of the points were used as training and 30% as validation to classify the entire PFT fractional cover dataset into a plant community map. Cluster selections were also informed by the spectral diversity calculation's requirement, described later, of using the same number of spectra from each community which limits the sample size of spectra used to the smallest community. Higher numbers of clusters results in additional smaller communities which are not well represented across all fires scars, and this limit spectra sample size and the representative ability of the spectral diversity calculation.

Table 2. Agglomerative coefficients of tested cluster linkage methods.

Linkage Method	Agglomerative Coefficient
Ward	0.998
Complete	0.965
Weighted	0.976
Average	0.951
Single	0.849

2.3 AVIRIS-NG DATA PREPARATION

Five AVIRIS-NG scenes were retrieved from the NASA JPL AVIRIS-NG Data Portal as orthocorrected radiance data with reflectance data (table 3). All flightlines were near cloud free, collected on August 8th, 2018. Topographic and BRDF corrections were applied to the imagery following the FlexBRDF method developed by Queally et al. (2022). Corrected imagery was then mosaicked in R, and the plant community map was downsampled to the AVIRIS-NG resolution and joined to the imagery. Several preprocessing steps were used to prepare the spectra for analysis. Similar to others (Laliberté et al., 2020; Badola et al., 2021), several groups

of "bad" bands were removed from our AVIRIS-NG product (table 4). Spectra were smoothed with a Savitzky-Golay filter which applies a polynomial fit to a filter window moved along each spectra, estimating the center of each window from the polynomial fit at that point, ultimately seeking to minimize least-squares error in fitting a polynomial to noisy spectra (Savitzky and Golay, 1964; Kienzle et al., 2021). A filter length of 7, and 3rd order polynomial fit was applied similar to Laliberté et al. (2020). This technique addresses spectral noise that could artificially inflate the measured spectral variability without overfitting and has been applied to AVIRIS-NG spectra in a variety of similar applications (Singh et al., 2021; Majeed et al., 2023). A polynomial order and filter width is provided and in this application a filter length of 7 and 3rd order polynomial fit was applied. NDWI was calculated and used to mask out water pixels from AVIRIS-NG data with values greater than 0.6, where all remaining pixels had their brightness normalized (equation 1).

Table 3. AVIRIS-NG Flightlines used.

Flight ID	Date	Site ID	Stated Pixel Size
ang20180818t194758	8/18/2018	AB_B10_L002_FL175_YKDelta	5.4m
ang20180818t200730	8/18/2018	AB_B10_L003_FL175_YKDelta	5.4m
ang20180818t203358	8/18/2018	AB_B10_L002_FL175_YKDelta	5.4m
ang20180818t205326	8/18/2018	AB_B10_L002_FL175_YKDelta	5.4m
ang20180818t211227	8/18/2018	AB_B10_L002_FL175_YKDelta	5.4m

Table 4. Removed AVIRIS-NG bands. Justifications adapted from Badola et al 2021 and Laliberte et al 2020.

Bands	Wavelength (nm)	Justification
1-6	376.86 – 401.9	Atmospheric scattering
194-214	1343.53 - 1443.71	Water vapor absorption bands
283-317	1789.3 - 1959.6	Water vapor absorption bands
405-425	2400.36 - 2500.54	Bands with poor radiometric calibration and absorption of water vapor and methane

$$normalized\ spectra = \frac{spectra}{\sqrt{\sum spectral\ bands^2}}$$

Equation 1. Normalization of AVIRIS-NG spectra.

2.4 SPECTRAL DIVERSITY CALCULATION

Spectral diversity was calculated using the functions published by Laliberté et al. (2020) with new alterations to accept predefined spatially heterogeneous communities as opposed to grid-defined communities. To compute the overall contribution of alpha and beta diversity to gamma diversity, we calculated spectral diversity independently for each fire scar and unburned area. The method, as it is based on the sum of squared spectral variance, requires that each community is represented with the same number of spectra, thus when communities are of different sizes, spectral diversity is calculated with a sample equal to the number of spectra in the smallest community, utilizing bootstrapping to obtain good representation of larger communities.

With large relative differences in community sizes within our study area (see table 6 in section 3.1) there were concerns that resulting sample sizes of spectra would be too small, which was a concern addressed in the following steps. Prior to calculating spectral diversity, communities accounting for less than 0.1% of the total fire scar or unburned area were filtered out of the analysis (see table 7 in section 3.1). Most of these removed communities were represented by approximately 100 AVIRIS-NG pixels or fewer. Next, all spectral diversity outputs were averaged across 50 bootstrap samples which minimized the standard deviation of endpoints. Resulting metrics from different areas were merged and used to reclassify the area and community layers to produce a rasterized spectral diversity product. In addition to the gamma, alpha, and beta diversities calculated, the feature and local contributions to spectral

diversity were calculated. The local contribution to beta diversity ($LCSD_{\beta}$) was calculated for each community, which finds the proportion of beta diversity each community contributed to therefore identifying which communities are more spectrally unique than others. The feature-specific contribution to spectral diversity (FCSD) identifies the proportion of total spectral variance contributed by each spectral feature, or band, for a given partition (alpha, beta, gamma) allowing for the understanding of which bands capture the most spectral diversity.

2.5 SURFACE SUBSIDENCE MAPPING

To examine possible relationships between wildfire, biodiversity, and permafrost degradation, estimating surface deformation using interferometric synthetic aperture radar (InSAR) at a resolution comparable to the community maps is advantageous to examine subsidence at large scale and with high resolution, where extensive fieldwork is not practical. Surface subsidence was mapped by estimating the annual surface deformation rate using interferogram pairs from Sentinel-1 C-band synthetic aperture radar (InSAR) at 60 m spatial resolution collected from post-fire 2015 to 2022 data acquired between mid-April to October (table 5). The estimate was calculated from the mean deformation rate over each thaw season. Thaw depth has been shown to follow a $NADDT^2$ dependence, where NADDT is the normalized accumulated degree days of thaw in a given thaw year (Hinkel and Nicholas, 1995). Therefore, the interferometric deformation rate from each pair can be thought of as a tangent line approximation to this curve (e.g., figure 2). These deformation rates were then averaged to derive an estimate of the seasonal subsidence deformation rate as a linear approximation to the NADDT curve for 2015-2021, as 2022 was shown to be an outlier with a late thaw season. The plant community map was resampled to match this resolution, and deformation rates were averaged within each community in each area. For further details on this product, see Michaelides and

Siegfried, though a summary of their InSAR processing is reproduced in figure 9 (2023). Additionally, soil moisture, surface saturation fraction, and active layer thickness estimates from an airborne SAR campaign were retrieved and similarly joined to the plant community map (Chen et al., 2022).

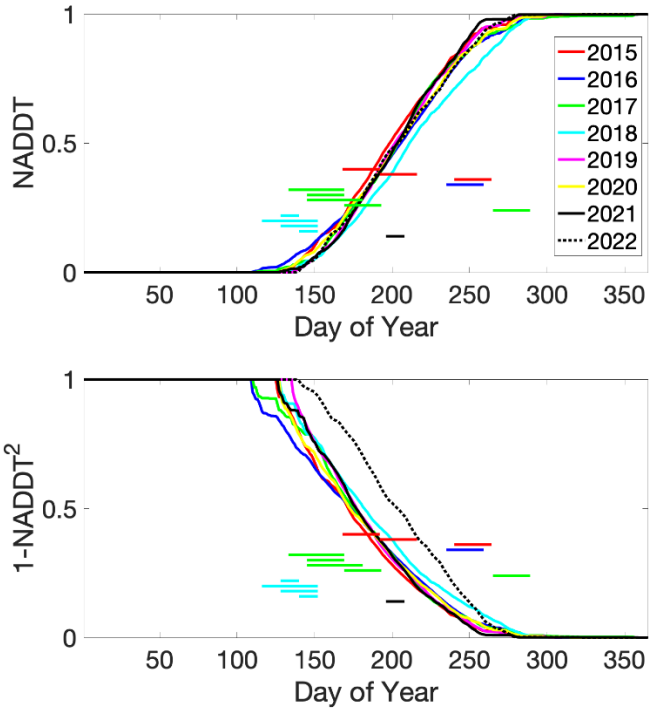

Figure 2. Normalized accumulated degree days of thaw (NADDT) and 1-NADDT^2 throughout the year estimated from Sentinel-1 interferometric pairs for 2015-2022. Time spans of interferometric pairs shown in horizontal bars, color coded with trend lines.

Table 5. List of Sentinel-1 interferometric pairs used in surface deformation analysis.

Interferometric Pair
20150617_20150711.int
20150711_20150804.int
20150828_20150921.int
20160822_20160915.int
20170513_20170618.int
20170525_20170618.int
20170525_20170630.int
20170618_20170712.int
20170922_20171016.int
20180508_20180520.int
20180426_20180601.int
20180508_20180601.int
20180520_20180601.int
20210715_20210727.int

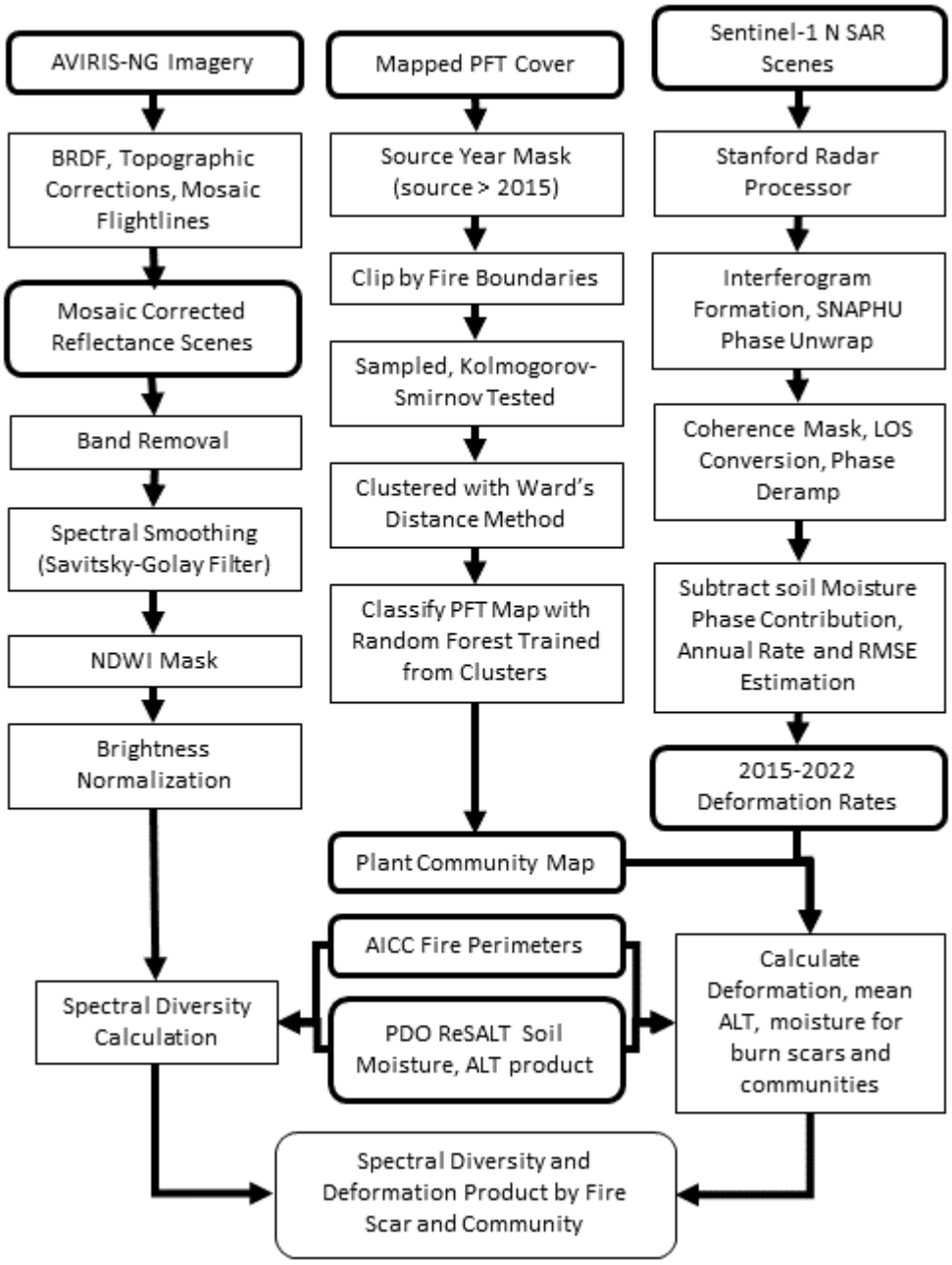

Figure 3. Process diagram for AVIRIS-NG imagery processing, plant community map creation, and InSAR methods reproduced from Michaelides and Siegfried (2023).

CHAPTER 3: RESULTS

3.1 PLANT COMMUNITY MAP

Hierarchical cluster analysis identified nine unique plant communities from the sample of 15,000 PFT fractional cover pixels, selecting a number of clusters past which there would be diminishing returns in the gap statistic (figures 4, 5). The sample and each points clustered community was used to classify the PFT fractional cover layers into the resulting plant community map (figure 6) with 70% of points used for training and 30% of points reserved for validation with an accuracy of 93% and kappa statistic of 0.93. The resulting communities were dominated largely by lichens, tussocks, dwarf shrubs, and tall shrubs. Shrub dominated communities cumulatively covered 54.8% of the study area and were generally more moist than others with overall mean surface saturation of 82%. Communities largely dominated by shrubs, evergreen, mixed, and deciduous, had little variation in soil moisture between burn scars (86%) and unburned areas (84%). Tussock tundras, occupying 7.1% of the study area, were the driest community with 58% soil saturation in burn scars and 50% in unburned areas, with graminoid tundras being the next driest at 77% in burn scars and 60% in unburned areas while covering 6.4% of the study area. Lichens were discriminated somewhat by moisture levels as the communities had similar cover proportions but slightly different soil moisture (60% dry, 63% moist-dry) and soil surface saturation (70% dry, 77% moist-dry).

Nine communities were produced through hierarchical cluster analysis by selecting a point along the gap-statistic plot that represented a point of diminishing returns with a higher number of clusters (figure 5). Plant communities included lichen dominated to shrub dominated tundra type which varied in stature, coverage, moisture, and deformation rates (table 6). Surface

soil saturation was also used to assist in the characterization of lichen communities that were similar in composition but varied in moisture (table 6, figure 7).

Plant community composition markedly varied within and among fire scars (figure 7). Unburned areas maintained high proportions of lichen tundra, whereas burn scars had a greater proportion of evergreen shrub-tussock and tussock-shrub tundra communities. Recent 2015 burn scars had mixed and evergreen shrub growth within 5 years after burn, though this growth was not observed in older scars. As time since burn increased, so also did the abundance of evergreen-shrub tussock communities, whereas moist-dry lichen communities remained in small amounts and drier lichen communities started to recover (e.g., POM, Long Lake, Dry Gulch, Water). Communities comprising less than 0.1% of cover in a fire scar or unburned area was removed to preserve the sample size of spectra used in the spectral diversity calculation (table 7).

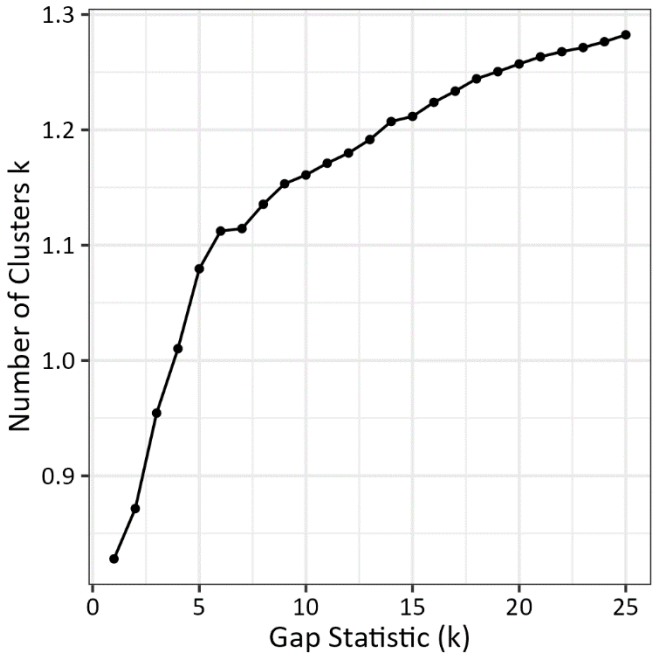

Figure 4. Gap-statistic of PFT fractional cover clustering at 1-25 clusters.

Table 6. Characteristics of mapped plant communities.

Tundra Plant Community	Percent of Study Area	Total Area (km^2)	Mean Soil Saturation at Surface (m^3/m^3, burn scar)	Mean Soil Saturation at Surface (m^3/m^3, unburned)	Mean Deformation (cm/day, burn scar)	Mean Deformation (cm/day, unburn scar)
Moist-Dry Lichen	18.5	144	0.83	0.67	-0.085	-0.067
Dry Lichen	13.1	102	0.83	0.65	-0.086	-0.067
Graminoid	6.4	50	0.77	0.60	-0.086	-0.068
Tussock	7.1	55	0.58	0.50	-0.081	-0.070
Tussock-Shrub	18.8	146	0.85	0.69	-0.076	-0.066
Evergreen Shrub-Tussock	15.7	122	0.85	0.68	-0.077	-0.066
Evergreen Shrub	7.5	50	0.90	0.93	-0.100	-0.096
Mixed Shrub	12.1	94	0.84	0.81	-0.096	-0.084
Deciduous Shrub	0.7	6	0.71	0.74	-0.072	-0.061

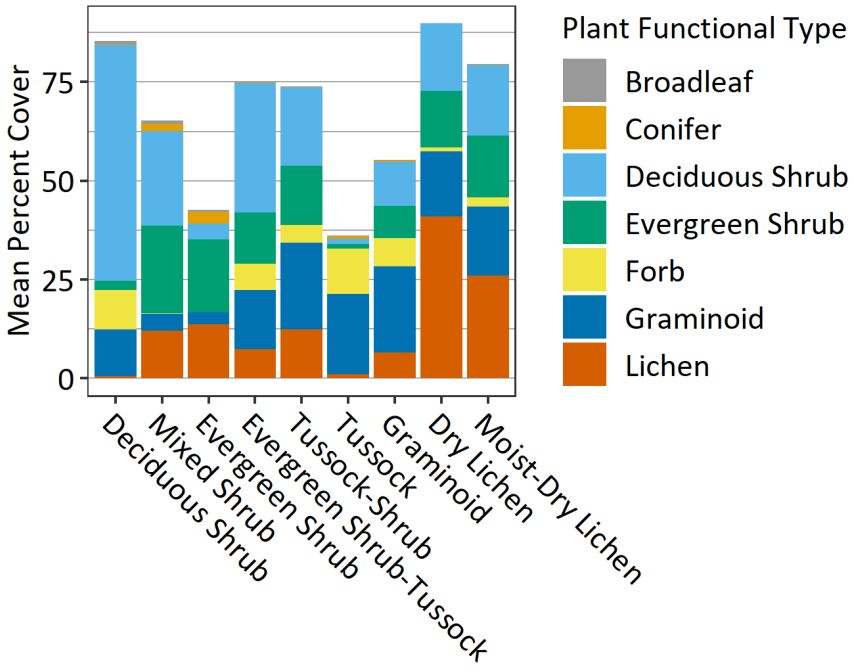

Figure 5. Plant functional type composition of hierarchically clustered tundra communities.

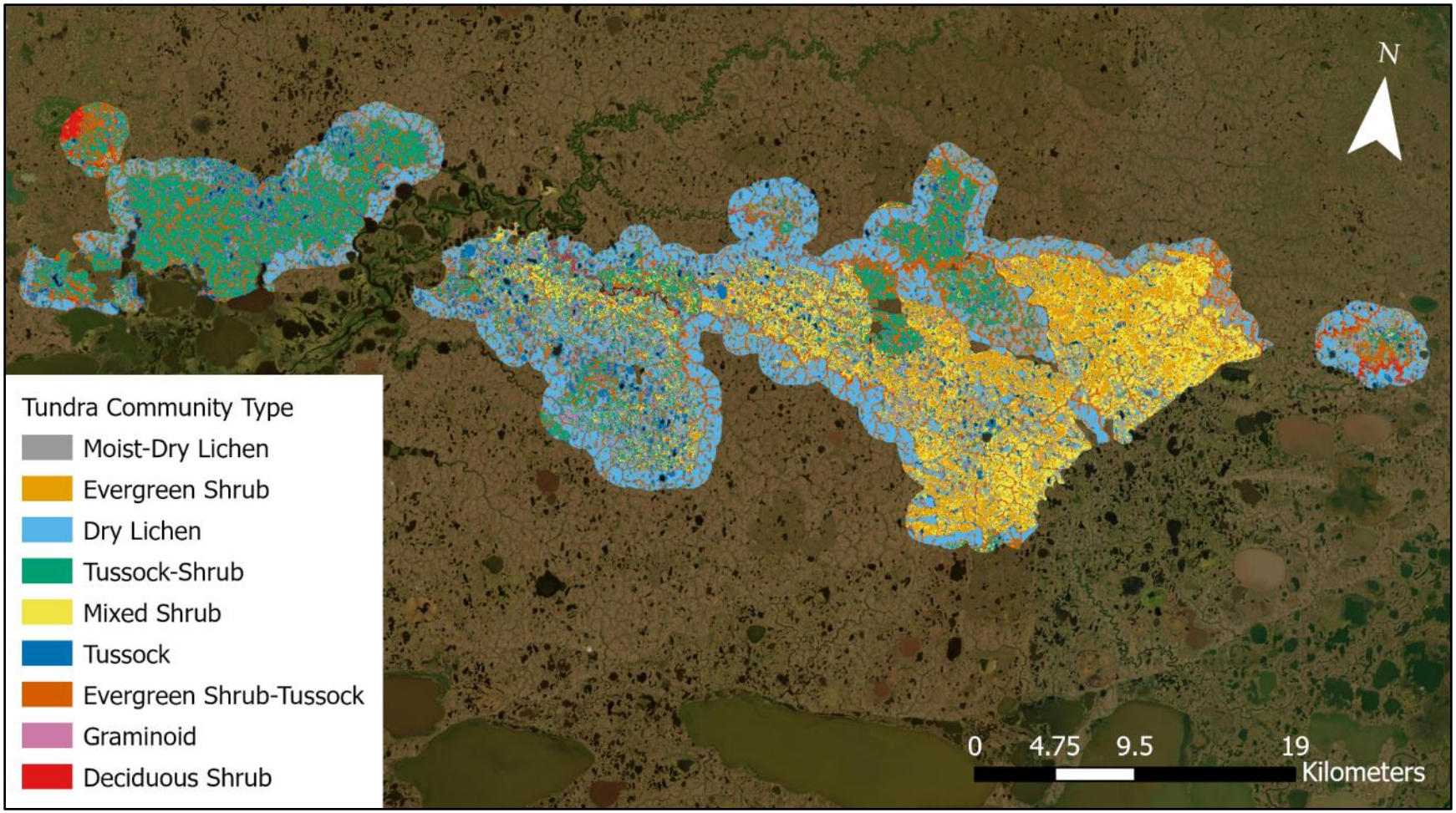

Figure 6. Plant Community Map at 1:375,000

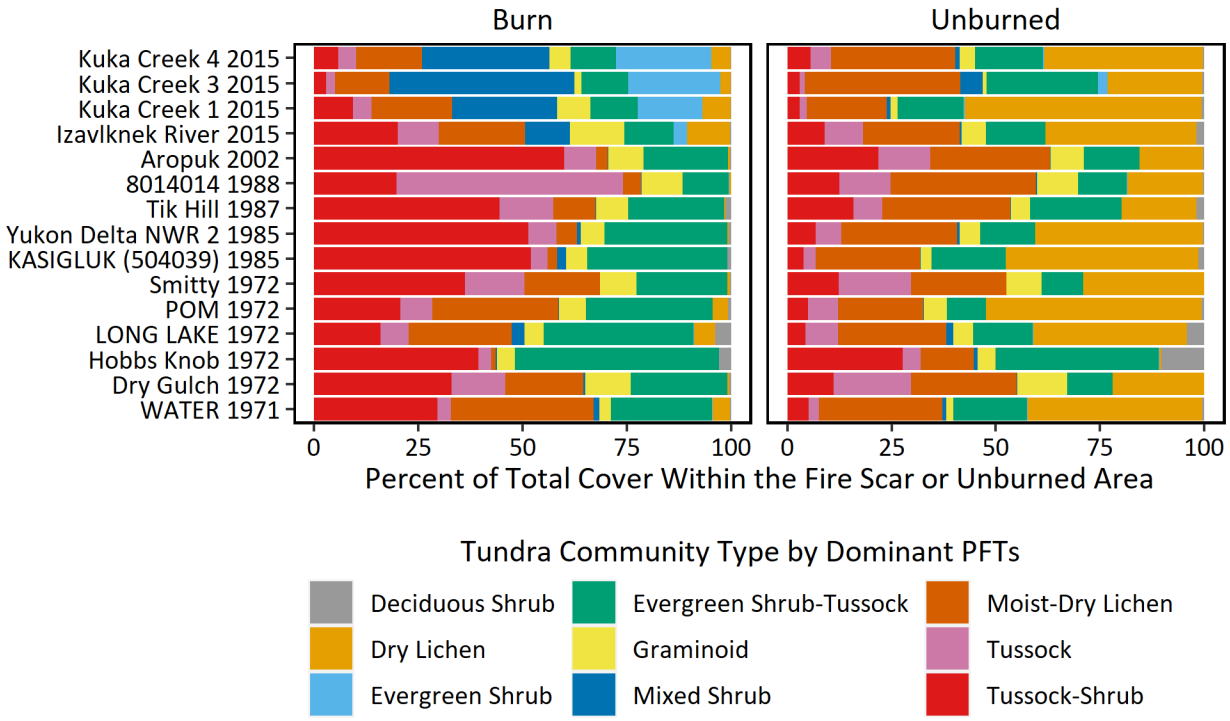

Figure 7. Proportion of community types in each burned and unburned area.

Table 7. Community occurrences cut from spectral diversity calculation due to small size.

Community	Area	Number of AVIRIS-NG Pixels	Percent of Area
Evergreen Shrub Tundra	8014014	30	0.079
Mixed Shrub Tundra	8014014	30	0.079
Mixed Shrub Tundra	Aropuk	2504	0.1
Evergreen Shrub Tundra	Aropuk (unburned)	146	0.012
Evergreen Shrub Tundra	Dry Gulch	59	0.052
Mixed Shrub Tundra	Dry Gulch (unburned)	161	0.1
Deciduous Shrub Tundra	Dry Gulch (unburned)	55	0.033
Evergreen Shrub Tundra	Hobbs Knob (unburned)	171	0.06
Evergreen Shrub Tundra	Izavlknek River (unburned)	112	0.018
Dry Lichen Tundra	KASIGLUK (504039)	35	0.008
Evergreen Shrub Tundra	KASIGLUK (504039) (unburned)	56	0.026
Deciduous Shrub Tundra	Kuka Creek 1	1114	0.091
Evergreen Shrub Tundra	POM (unburned)	86	0.026
Mixed Shrub Tundra	Smitty	55	0.028
Mixed Shrub Tundra	Smitty (unburned)	113	0.059
Deciduous Shrub Tundra	Smitty (unburned)	123	0.059
Evergreen Shrub Tundra	Tik Hill	86	0.029
Evergreen Shrub Tundra	Tik Hill (unburned)	25	0.014
Mixed Shrub Tundra	Tik Hill (unburned)	165	0.082
Evergreen Shrub Tundra	WATER	115	0.016
Evergreen Shrub Tundra	WATER (unburned)	274	0.1
Evergreen Shrub Tundra	Yukon Delta NWR 2 (unburned)	96	0.051

3.2 FIRE-SCALE SPECTRAL DIVERSITY

We found a strong positive correlation between gamma diversity and time since fire (R^2 = 0.74, $p < 0.001$, figure 8), and this strong statistical effect of time since fire also held for alpha diversity (R^2 = 0.79, $p < 0.001$), but not with beta diversity (R^2 = 0.16, p = 0.01). With the exception of the two recent 2015 fires, a pairwise examination (i.e., paired t-test) shows a greater gamma diversity in the unburned areas versus the burn scars, with a mean difference of -0.00185 ($p < 0.001$). The partitioning of alpha and beta spectral diversities revealed on average 72% of

gamma spectral diversity across fires was attributed to alpha diversity, with the rest attributable to beta diversity, though there was no significant relationship between the partition proportion and burn scar age nor significant difference of partition proportion between burn scars and paired unburned areas (figure 9).

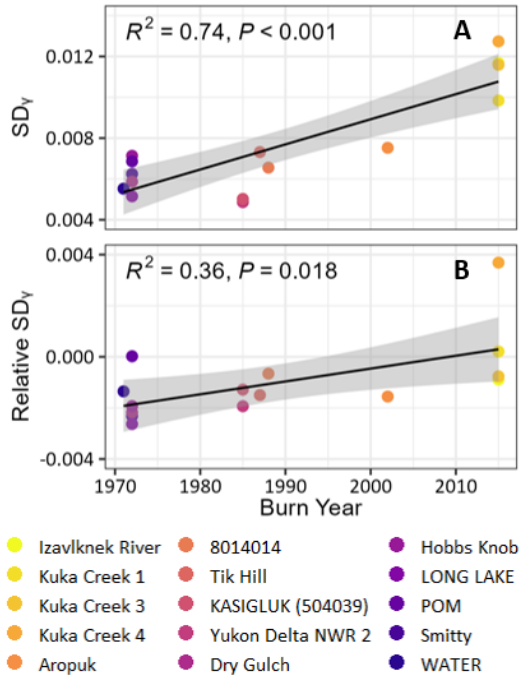

Figure 8. Gamma spectral diversity (A) and relative gamma spectral diversity compared to unburned (B) of each burn scar. Each area's gamma diversity is calculated using up to 4.35 million AVIRIS-NG pixels depending on the size of the area (see section 2.3).

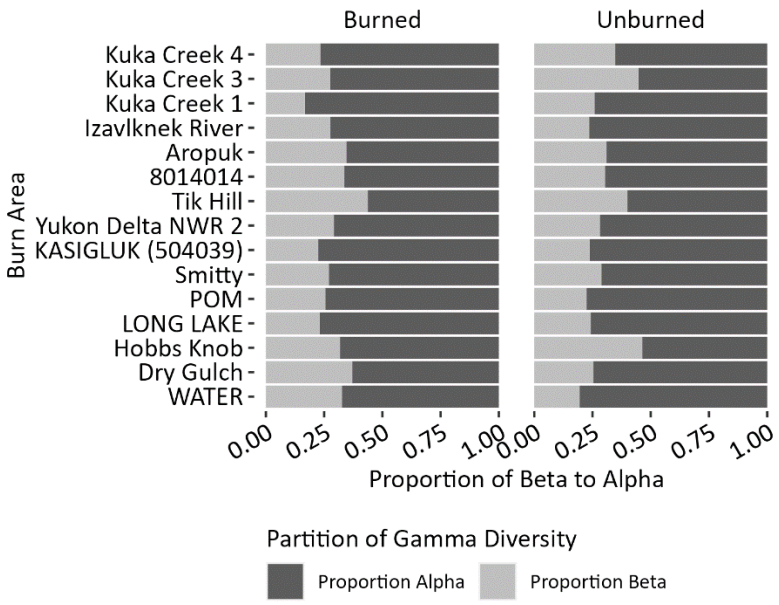

Figure 9. Proportion of alpha to beta spectral diversity when partitioned from gamma.

3.3 COMMUNITY LEVEL DIVERSITY METRICS

Alpha diversity was highest in tussock and graminoid dominated communities, while all shrub dominated communities' diversity was in a consistent range between about 0.01 and 0.0025. Lichen dominated communities had the lowest alpha diversity, generally below 0.005. Unburned communities had higher alpha diversity, generally following the fire scar-level trends, except dry lichen communities which had lower alpha diversity within unburned areas (0.0016) compared to burn scars (0.0023). The patterns of $LCSD_{\beta}$ among communities were similar within two groups, where deciduous shrub, evergreen shrub, dry lichen, and tussock communities had higher contributions (20 - 30 % on average) and greater variability, while all others had low (generally <15% on average) and consistent $LCSD_{\beta}$ (figure 12).

FCSD at the individual fire level was consistent between gamma, beta, and mean alpha diversity, and almost all burn scars had similar FCSD curves across all wavelengths. FCSD alpha ($FCSD_{\alpha}$) values of each community demonstrate elevated importance within the red-edge, NIR,

and different portions of the SWIR (1300 - 1350 nm, 1450 - 1800 nm) and was generally low in the visible spectrum and portions of the SWIR range (950 - 1000 nm, 1150 - 1250 nm, 2300 - 2400 nm, figure 11). Tussock and graminoid communities were consistent exceptions to this trend, as they had high importance in the visible range and decreased importance within the NIR and SWIR ranges of 1450 nm and higher. Recent 2015 fires all showed consistent alpha diversities between burn scars and corresponding unburned areas, and a paired t-test of all (figure 10). However, fire scars older than 15 years since burn showed significantly lower alpha diversities (mean difference of -0.0014, $p < 0.001$) than their unburned counterparts.

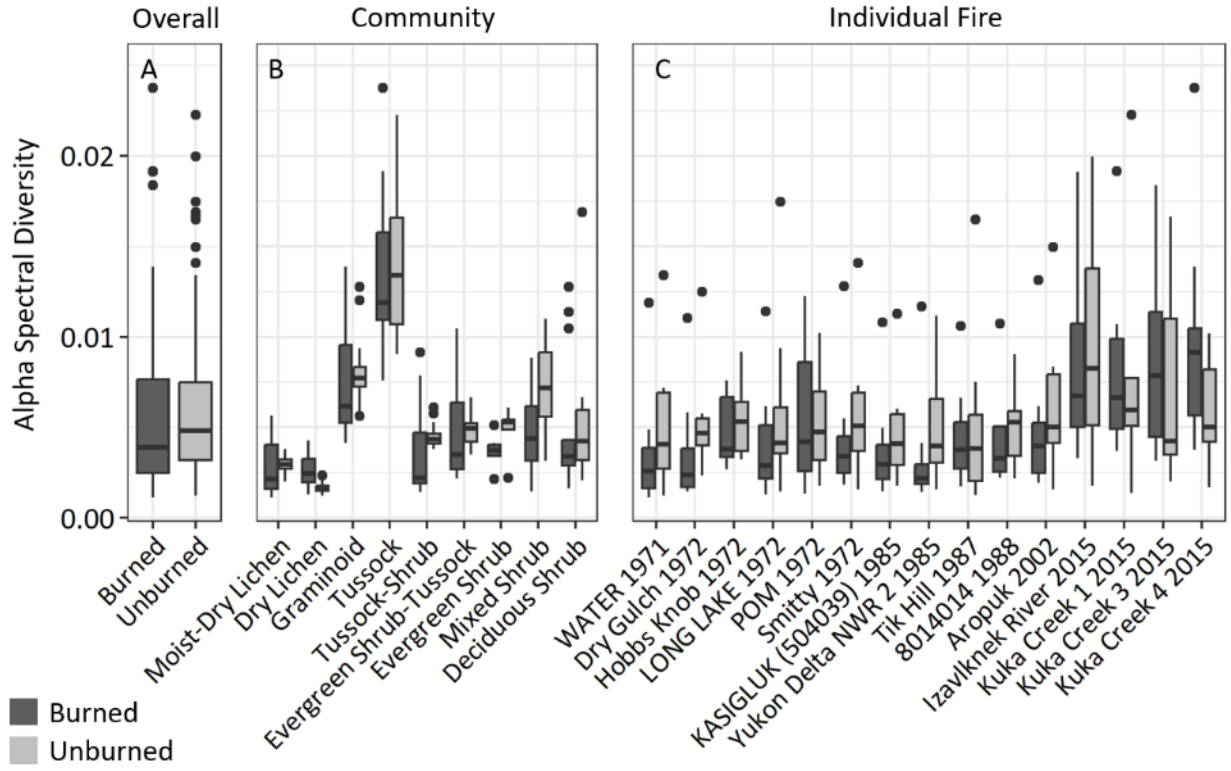

Figure 10. Alpha Spectral Diversity organized at the region (A), community (B), and area (C) scales.

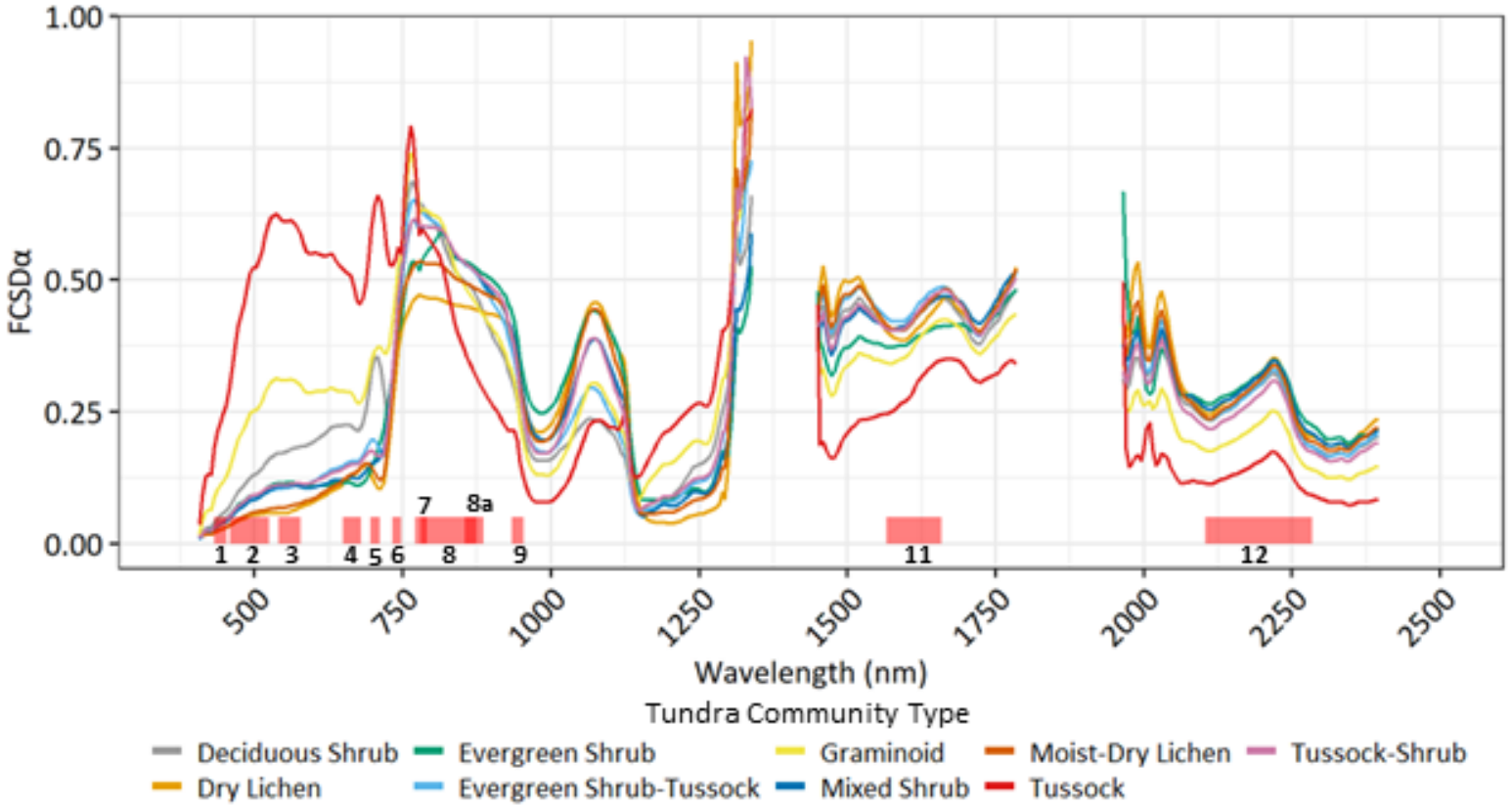

Figure 11. Feature-specific contribution to alpha diversity showing relative percent importance of each wavelength to spectral diversity by community type with selected Sentinel-2 MSI bands overlaid. Higher values indicate a wavelength accounted for more spectral variation than others.

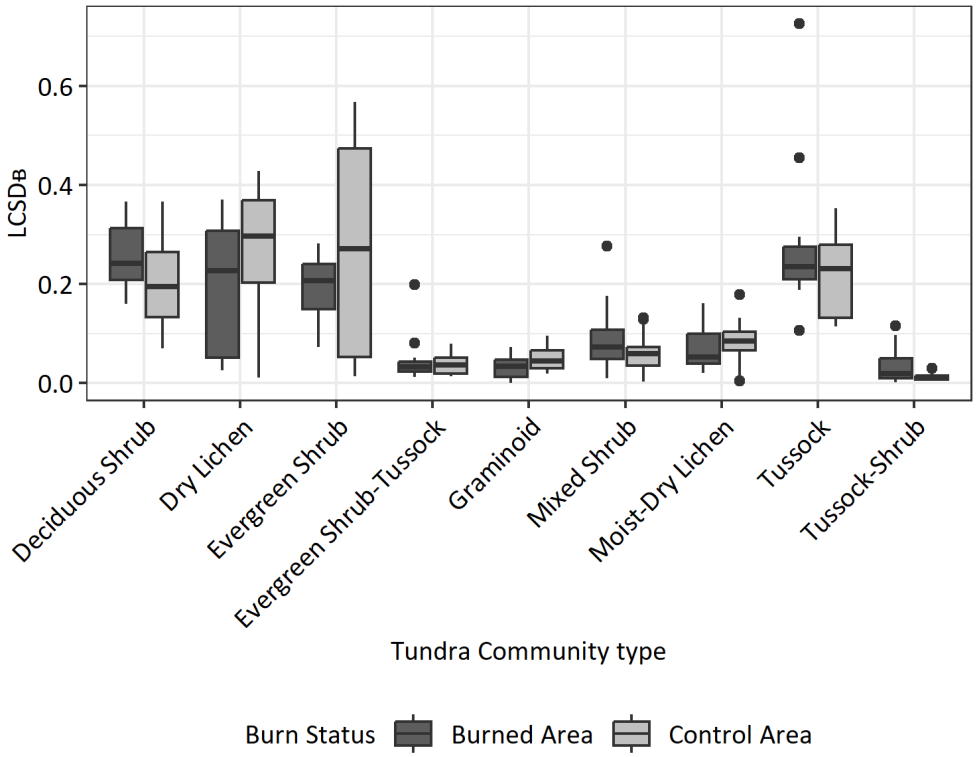

Figure 12. Local contribution to beta spectral diversity between communities showing the relative proportion of total spectral variance each community contributed to beta diversity.

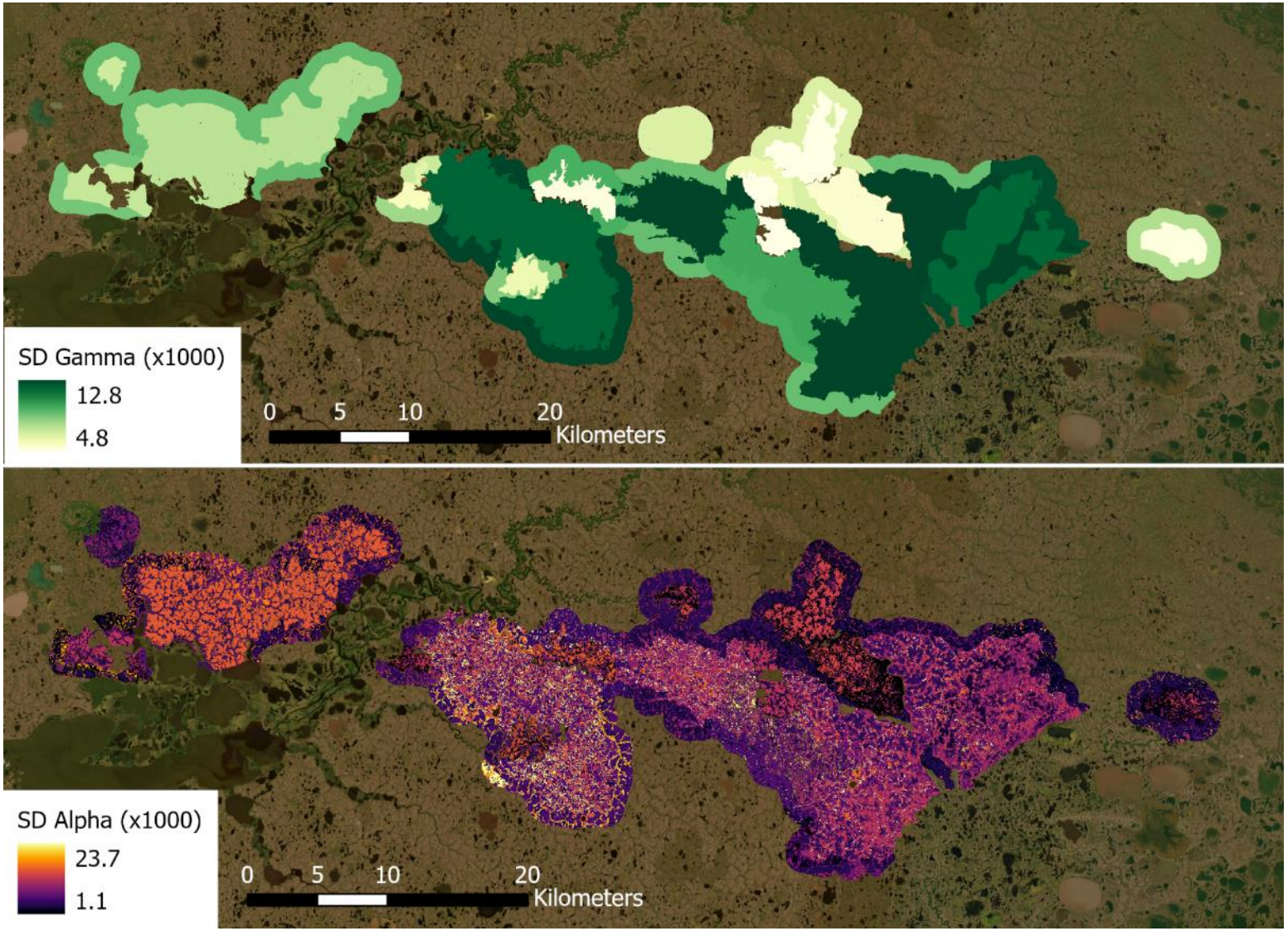

Figure 13. Gamma (upper) and alpha (lower) spectral diversity mapped across burn scars and communities within.

3.4 DIVERSITY AND SUBSIDENCE INTERACTIONS

Surface deformation was found to be significantly higher in magnitude within burn scars than paired unburned areas when examined with a paired student's t-test (mean difference -0.007 cm day^{-1}, $p = 0.01$). Among community types, deformation rates were highly variable particularly amongst communities in burn scars, for example mixed shrub communities in burn scars had deformation range from -0.07 cm day^{-1} to -0.1 cm day^{-1} due to the strong burn-age relationship with deformation rates (figure 14). Evergreen shrub communities and to a lesser extent mixed shrub communities had the highest deformation rates, considering that evergreen and mixed shrubs mostly occurred in fire scars from 2015 with little presence on the landscape in other scars and unburned areas. However most other communities had similar means and spread of deformation rates as they are heavily influenced by fire scar age. Surface subsidence's relationship with burn scar age was strong ($R^2 = 0.75$, $p < 0.001$), where recent fire scars had higher deformation rates relative to their unburned counterparts than older fire scars ($R^2 = 0.87$, $p < 0.001$, figures 14, 15). Burn scars older than 15 years had a reduced difference between fire scar and unburned area deformation compared to recent burn scars (mean difference of -0.0014 cm day^{-1}, older, vs -0.0176 cm day^{-1}, recent). Deformation was strongly correlated with gamma spectral diversity ($R^2 = 0.63$, $p < 0.001$) and mean alpha spectral diversity ($R^2 = 0.74$, $p < 0.001$) of fire scars, and these patterns were consistent with active layer thickness ($R^2 = 0.61$, $p < 0.001$). This deepening of active layers had weaker correlations with gamma ($R^2 = 0.35$, $p = 0.01$) and mean alpha diversity ($R^2 = 0.47$, $p = 0.003$) than subsidence.

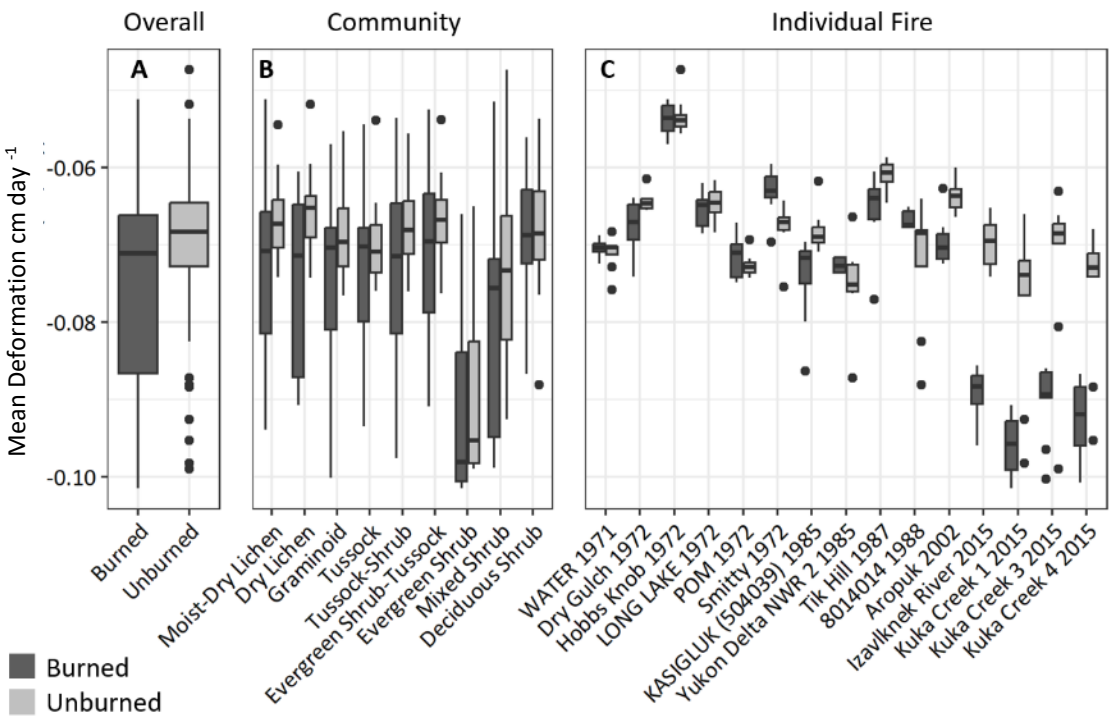

Figure 14. Surface deformation of communities grouped by burn status alone (A), community type (B), and individual fires (C) sorted by burn year.

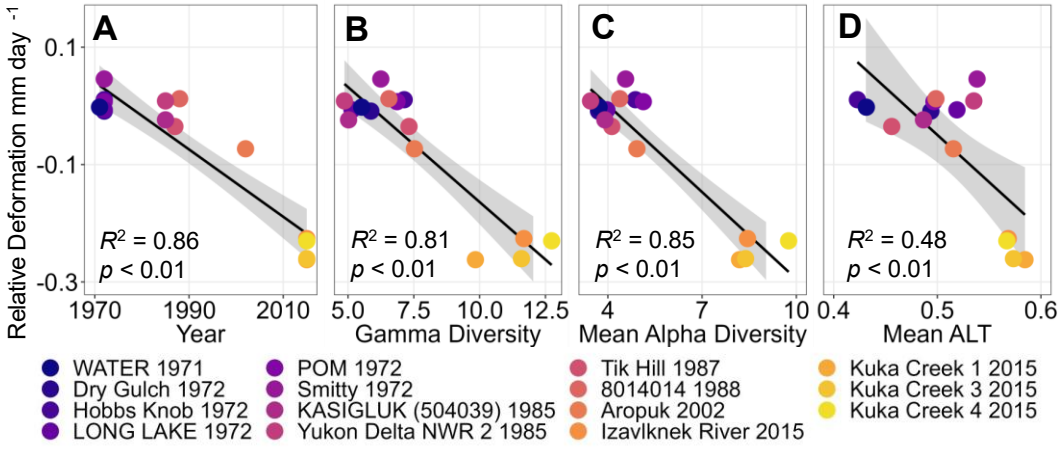

Figure 15. Relative surface deformation between burned and unburned pairs correlated with year of burn (A), gamma spectral diversity (B), mean alpha diversity (C), and mean active layer thickness (D).

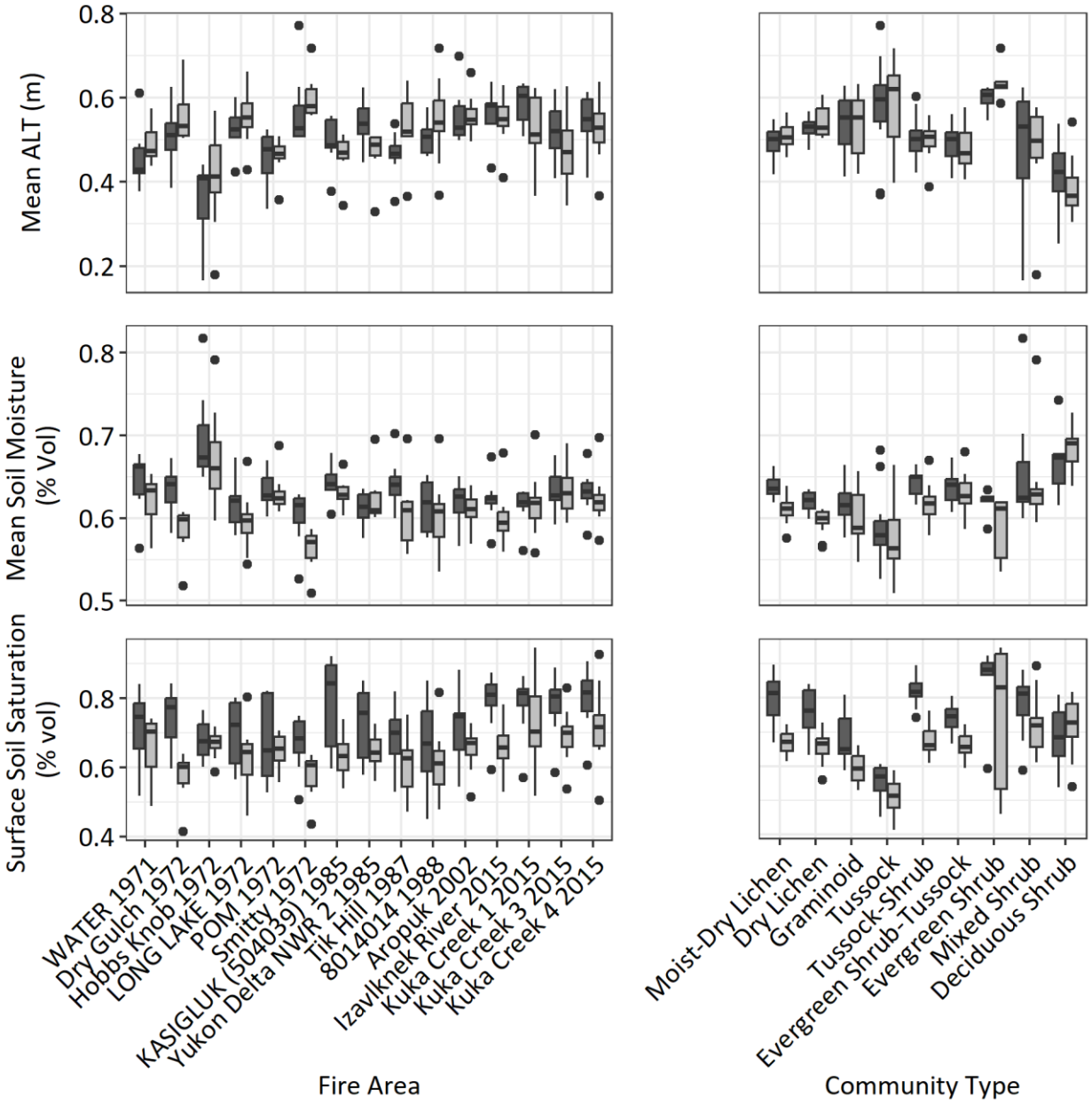

Figure 16. Remotely sensed environmental variables active layer thickness, soil moisture though the active layer, and surface soil saturation fraction at the community level shown organized by burn and by community, separated by burn or unburned status (Chen et al., 2022).

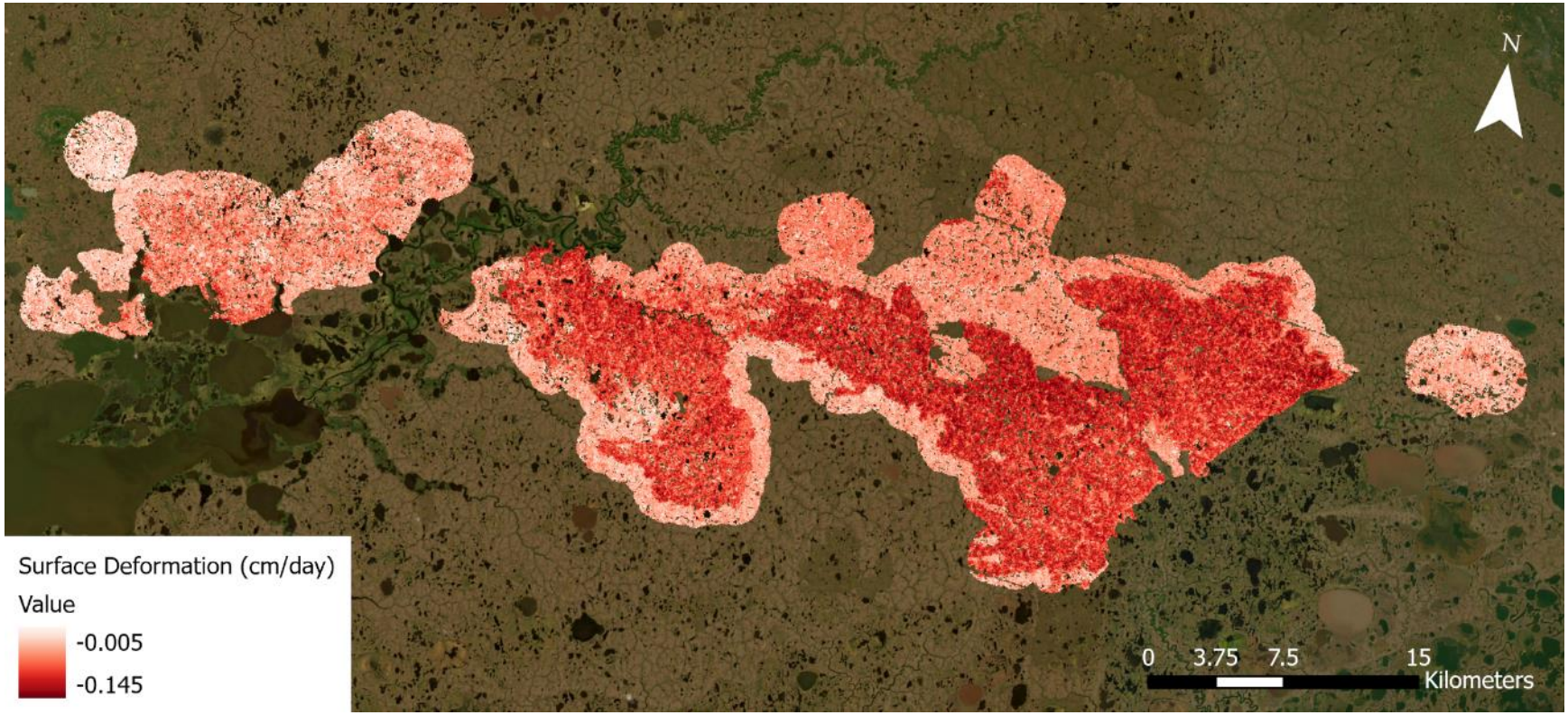

Figure 17. 2015-2022 InSAR-derived surface deformation rate across fire scars and unburned reference areas.

CHAPTER 4: DISCUSSION AND CONCLUSIONS

4.1 SPECTRAL DIVERSITY AND DEFORMATION INTERACTIONS

The effects of 47 years of tundra fires on the YK Delta resulted in major ecological changes in the distribution of plant functional types, surface subsidence, and spectral diversity metrics. Our plant community maps describe similar spatiotemporal patterns from that reported by ground-based post-fire vegetation succession observations (Frost et al., 2020). Spatial community products also identify a reduction in lichen cover and increase in shrub cover relative to unburned terrain, with evergreen shrub-tussock and tussock-shrub communities becoming dominant in burn scars older than 15 years. Overall, we identified multiple shrub-dominated communities to exhibit lower alpha diversities than lichen, graminoid and tussock dominated communities. This is potentially due to differences in the similarity in canopy structure between shrubs and smaller species, which can occupy larger portions of spectral signal (Nelson et al., 2022). Therefore, due to the prevalence of shrub communities across the IKU, we anticipate a reduction in spectral diversity of burn scars over time, likely reducing the biodiversity of the tundra per unit area.

Although it is challenging to link the observed short and long-term responses of spectral diversity to fire and surface subsidence without controlling for multiple interacting factors (e.g., plant species replacement, soil moisture, soot deposition), our analysis suggests that spectral diversity is indeed negatively related to time since fire and positively related to surface subsidence. Tundra fires on the IKU removed or disturbed lichen dominated tundra, enabling the pervasive shift in shrub dominance over time. Our burn chronosequence indicates over 2-3 years following fire, spectral diversity and surface subsidence rapidly increased then declined and stabilized after ~20 years. These patterns in PFT cover and resulting spectral diversities are in

line with Frost et al. (2020), which found increases in evergreen shrubs, deciduous shrubs, and graminoid species in recent burn scars as lichens decreased relative to unburned areas, which likely increased spectral variation. The strong relationship between both alpha and gamma diversities and burn age, along with the high proportion of alpha diversity contribution to gamma estimates suggest observed diversity trends over time are highly dependent on alpha diversity. Though surface char and soot following fire may have increased the spectral diversity, we think this effect was reduced through masking out area with no vegetative cover from the PFT data, and as we still identified a significant correlation between fire scar age and gamma diversity, including normalized gamma diversity using unburned reference areas (figure 8). Therefore, spectral diversity was likely primarily driven by post-fire vegetation succession interacting with thickening active layers and surface deformation which for example can change local moisture regimes resulting in higher surface water saturation, making environmental conditions more favorable for sedges and grasses (graminoid dominated communities).

4.2 SPECTRAL DIVERSITY APPLICATION AND UNCERTAINTY

Our use of a plant community map from clustered PFT cover is advantageous in remote regions as spectral diversity describes potential differences in measured plant cover within communities; thus inferences can be made upon community ecology from such spectral diversity metrics. Most previous assessments of spectral diversity have used uniform gridded communities drawn across study sites, in similar size to sampling plots in traditional ecology. This allows for quick community delineations when there is little spatial data to characterize species or functional type composition across the study area, but these communities are often arbitrary and would require additional field or image interpretation work to characterize such numerous plot-style communities. However, there are some limitations and sources of uncertainty to our

method. A specific limitation of applying spectral diversity to a chronosequence of fire scars is recently burned areas can have artificially high spectral diversity from the inclusion of lower-reflectance spectra from burn char or similarly darkened vegetation. This was mitigated by three growing seasons occurring between burn and imagery collection and by applying a bare ground zero PFT cover mask and a NDWI mask, after which an NDVI mask was considered, though remaining pixels had high NDVI values across area, and an appropriate 0.2 mask had little alterations to the imagery and resulting spectral metrics. It is possible that higher spatial resolutions would experience this issue to a greater degree as remaining char amongst healthy vegetation could be isolated to represent the majority of pixels.

Further efforts to apply spectral diversity to examine disturbances like fire would help refine how to handle spectral variance from non-vegetated cover. A broader challenge of applying spectral diversity methods which rely on spectral variability is the sensor-dependency of results as each spectra can be dependent on sensor, calibration, processing, and time of acquisition (Wang and Gamon, 2019). This is particularly present where high resolution, but low spatial coverage aerial and drone imagery may not be spectrally harmonized between scenes from the same sensor and have other artefacts between time-separate scenes covering the same area. By expanding work in comparing spectral diversity across space (Schmidtlein, 2017) and time (Rossi et al., 2021) better methods can be developed to better apply spectral diversity to environmental disturbances where comparisons across a time-series and/or different sites are desired.

4.3 CONCLUSIONS

Tundra regions are experiencing rapid climate and environmental change that is influencing the prevalence of permafrost thaw and surface subsidence and wildfire occurrence,

with implications for plant community composition. Spectral diversity approximates species diversity and associated plant productivity metrics similar to functional and phylogenetic diversity which enables us to uncover new insights into interactions among ecological disturbances in permafrost regions (Rocchini et al., 2010; Schweiger, 2018). Along our burn scar chronosequence we found recent scars to have higher gamma (total) spectral diversity and surface subsidence, while in burn scars older than 15 years, deformation and gamma diversity reduced over time, resulting in subsidence similar to unburned areas and gamma diversity lower than unburned areas. We suggest that increased spectral diversity in recent burn scars is due primarily to a wider diversity of species attempting to recolonize and is partly driven by increased post-burn subsidence which thickens the active layer.

Improved and spectrally consistent hyperspectral data collection on aerial platforms could facilitate examining spectral diversity at different timesteps and between different areas. Upcoming missions such as the Planet hyperspectral Tanager satellites and NASA's Surface Biology and Geology (SBG) will allow new approaches to examining spectral diversity with a high input of spectral species at moderate resolution and large scale, which can be particularly advantageous for expansive remote areas in the arctic and sub-arctic. Improvements to spectral diversity application will aid mapping of biodiversity and examinations of community response to disruptions and aid insight into ecosystem functions.

REFERENCES

ACRC (Alaska Climate Research Center). (2023). Precipitation Normals for Bethel Airport, AK, 1981-2010. Accessed October 2023. (https://akclimate.org/data/precipitation-normals/).

AICC (Alaska Interagency Coordination Center). (2023). Fire History Perimeters. Accessed February 2023. (https://fire.ak.blm.gov/arcgis/rest/services/MapAndFeatureServices/FireHistory/FeatureServer).

Badola, A., Panda, S. K., Roberts, D. A., Waigl, C. F., Bhatt, U. S., Smith, C. W., & Jandt, R. R. (2021). Hyperspectral Data Simulation (Sentinel-2 to AVIRIS-NG) for Improved Wildfire Fuel Mapping, Boreal Alaska. *Remote Sensing*, 13(9), 1693.

Carlson, K. M., Asner, G. P., Hughes, R. F., Ostertag, R., & Martin, R. E. (2007). Hyperspectral Remote Sensing of Canopy Biodiversity in Hawaiian Lowland Rainforests. *Ecosystems*, *10*(4), 536–549.

Chaurasia, A. N., Dave, M. G., Parmar, R. M., Bhattacharya, B., Marpu, P. R., Singh, A., & Krishnayya, N. S. R. (2020). Inferring Species Diversity and Variability over Climatic Gradient with Spectral Diversity Metrics. *Remote Sensing*, *12*(13), 2130.

Chen, R.H., R.J. Michaelides, J. Chen, A.C. Chen, L.K. Clayton, K. Bakian-Dogaheh, L. Huang, E. Jafarov, L. Liu, M. Moghaddam, A.D. Parsekian, T.D. Sullivan, A. Tabatabaeenejad, E. Wig, H.A. Zebker, and Y. Zhao. (2022). ABoVE: Active Layer Thickness from Airborne L- and P- band SAR, Alaska, 2017, Ver. 3. ORNL DAAC, Oak Ridge, Tennessee, USA.

Chipman, M. L., Hudspith, V., Higuera, P. E., Duffy, P. A., Kelly, R., Oswald, W. W., & Hu, F. S. (2015). Spatiotemporal patterns of tundra fires: Late-Quaternary charcoal records from Alaska. *Biogeosciences*, *12*(13), 4017–4027.

Dahlin, K. M. (2016). Spectral diversity area relationships for assessing biodiversity in a wildland–agriculture matrix. *Ecological Applications*, *26*(8), 2758–2768.

Féret, J.-B., & Asner, G. P. (2014). Mapping tropical forest canopy diversity using high-fidelity imaging spectroscopy. *Ecological Applications*, *24*(6), 1289–1296.

French, N. H. F., Jenkins, L. K., Loboda, T. V., Flannigan, M., Jandt, R., Bourgeau-Chavez, L. L., & Whitley, M. (2015). Fire in arctic tundra of Alaska: Past fire activity, future fire potential, and significance for land management and ecology. *International Journal of Wildland Fire*, 24(8), 1045.

Frost, G. V., Loehman, R. A., Saperstein, L. B., Macander, M. J., Nelson, P. R., Paradis, D. P., & Natali, S. M. (2020). Multi-decadal patterns of vegetation succession after tundra fire on the Yukon-Kuskokwim Delta, Alaska. Environmental Research Letters, 15(2), 025003.

Gholizadeh, H., Gamon, J. A., Townsend, P. A., Zygielbaum, A. I., Helzer, C. J., Hmimina, G. Y., Yu, R., Moore, R. M., Schweiger, A. K., & Cavender-Bares, J. (2019). Detecting prairie biodiversity with airborne remote sensing. *Remote Sensing of Environment*, *221*, 38–49.

Gill, R.E.J., Handel, C.M. (1990). The importance of subarctic intertidal habitats to shorebirds: A study of the central Yukon-Kuskokwim Delta, Alaska. *The Condor*, 92, 709-725.

Hall, D. K., V. V. Salomonson, and G. A. Riggs. 2016. MODIS/Terra Snow Cover Daily L3 Global 500m Grid. Version 6. Boulder, Colorado USA: NASA National Snow and Ice Data Center Distributed Active Archive Center.

Hinkel, K. M., & Nicholas, J. R. J. (1995). Active Layer Thaw Rate at a Boreal Forest Site in Central Alaska, U.S.A. *Arctic and Alpine Research*, *27*(1), 72.

Hu, F. S., Higuera, P. E., Duffy, P., Chipman, M. L., Rocha, A. V., Young, A. M., Kelly, R., & Dietze, M. C. (2015). Arctic tundra fires: Natural variability and responses to climate change. *Frontiers in Ecology and the Environment*, *13*(7), 369–377.

Iwahana, G., Uchida, M., Liu, L., Gong, W., Meyer, F., Guritz, R., Yamanokuchi, T., & Hinzman, L. (2016). InSAR Detection and Field Evidence for Thermokarst after a Tundra Wildfire, Using ALOS-PALSAR. *Remote Sensing*, *8*(3), 218.

Jacobs, P., Lenssen, N., Schmidt, G., & Rohde, R. (2021, December 13-17). *The Arctic Is Now Warming Four Times As Fast As the Rest of the Globe*. [Conference Presentation]. AGU Fall Meeting 2021, held in New Orleans, LA, United States. id A13E-02.

Jha, C. S., Rakesh, Singhal, J., Reddy, C. S., Rajashekar, G., Maity, S., Patnaik, C., Das, A., Misra, A., Singh, C. P., Mohapatra, J., Krishnayya, N. S. R., Kiran, S., Townsend, P., & Martinez, M. H. (2019). Characterization of Species Diversity and Forest Health using AVIRIS-NG Hyperspectral Remote Sensing Data. *Current Science*, *116*(7), 1124.

Jones, B. M., Grosse, G., Arp, C. D., Miller, E., Liu, L., Hayes, D. J., & Larsen, C. F. (2015). Recent Arctic tundra fire initiates widespread thermokarst development. *Scientific Reports*, 5(1), 15865.

Jorgenson, M., Frost, G., & Dissing, D. (2018). Drivers of Landscape Changes in Coastal Ecosystems on the Yukon-Kuskokwim Delta, Alaska. *Remote Sensing*, *10*(8), 1280.

Kacic, P., & Kuenzer, C. (2022). Forest Biodiversity Monitoring Based on Remotely Sensed Spectral Diversity—A Review. *Remote Sensing*, *14*(21), 5363.

Kienzle, P., Ligges, U., & Short, T. (2021). Package “signal” (0.7-7) [R package].

Laliberté, E., Schweiger, A. K., & Legendre, P. (2020). Partitioning plant spectral diversity into alpha and beta components. *Ecology Letters*, 23(2), 370–380.

Liu, L., Schaefer, K. M., Chen, A. C., Gusmeroli, A., Zebker, H. A., & Zhang, T. (2015). Remote sensing measurements of thermokarst subsidence using InSAR. *Journal of Geophysical Research: Earth Surface*, *120*(9), 1935–1948.

Macander, M.J., & Nelson, P.R. (2022). *Arctic-Boreal Vulnerability Experiment (ABoVE)ABoVE: Modeled Top Cover by Plant Functional Type over Alaska and Yukon, 1985-2020* [GTiff].

Mackay, J. R. (1995). Active Layer Changes (1968 to 1993) Following the Forest-Tundra Fire near Inuvik, N.W.T., Canada. *Arctic and Alpine Research*, *27*(4), 323.

Maechler, M., Rousseeuw P, Struyf A, Hubert M, Hornik K (2022). cluster: Cluster Analysis Basics and Extensions. (2.1.4) [R Package].

Majeed, I., Purushothaman, N. K., Chakraborty, P., Panigrahi, N., Vasava, H. B., & Das, B. S. (2023). Estimation of soil and crop residue parameters using AVIRIS-NG hyperspectral data. *International Journal of Remote Sensing*, *44*(6), 2005–2038.

McCune, B., & Grace, J. B. (2002). Analysis of Ecological Communities. In *Analysis of Ecological Communities* (pp. 86–97). MjM Software Design.

McPartland, M., Falkowski, M., Reinhardt, J., Kane, E., Kolka, R., Turetsky, M., Douglas, T., Anderson, J., Edwards, J., Palik, B., & Montgomery, R. (2019). Characterizing Boreal Peatland Plant Composition and Species Diversity with Hyperspectral Remote Sensing. *Remote Sensing*, *11*(14), 1685.

Michaelides, R. J., and Siegfried, M. R. (2023). Studying Permafrost-Wildfire Interactions in the Age of NISAR. *2023 IEEE International Geoscience & Remote Sensing Symposium Proceedings*, Pasadena, California, July 16th - July 21st, 2023.

Michaelides, R. J., Schaefer, K., Zebker, H. A., Parsekian, A., Liu, L., Chen, J., Natali, S., Ludwig, S., & Schaefer, S. R. (2019). Inference of the impact of wildfire on permafrost and active layer thickness in a discontinuous permafrost region using the remotely sensed active layer thickness (ReSALT) algorithm. *Environmental Research Letters*, 14(3), 035007.

MTBS Project (USDA Forest Service/U.S. Geological Survey) (2023). Data Access: Fire Level Geospatial Data. Accessed September 2023. (https://mtbs.gov/direct-download).

Murtagh, F., & Legendre, P. (2014). Ward's Hierarchical Agglomerative Clustering Method: Which Algorithms Implement Ward's Criterion? *Journal of Classification*, *31*(3), 274–295.

Nelson, P. R., Maguire, A. J., Pierrat, Z., Orcutt, E. L., Yang, D., Serbin, S., Frost, G. V., Macander, M. J., Magney, T. S., Thompson, D. R., Wang, J. A., Oberbauer, S. F., Zesati, S. V., Davidson, S. J., Epstein, H. E., Unger, S., Campbell, P. K. E., Carmon, N., Velez-Reyes, M., & Huemmrich, K. F. (2022). Remote Sensing of Tundra Ecosystems Using

High Spectral Resolution Reflectance: Opportunities and Challenges. *Journal of Geophysical Research: Biogeosciences, 127*(2), e2021JG006697.

Nowacki, Gregory; Spencer, Page; Fleming, Michael; Brock, Terry; and Jorgenson, Torre. Ecoregions of Alaska: 2001. U.S. Geological Survey Open-File Report 02-297.

Osterkamp, T. E., Jorgenson, M. T., Schuur, E. A. G., Shur, Y. L., Kanevskiy, M. Z., Vogel, J. G., & Tumskoy, V. E. (2009). Physical and ecological changes associated with warming permafrost and thermokarst in Interior Alaska: Physical and Ecological Changes Associated with Thermokarst. *Permafrost and Periglacial Processes,* 20(3), 235–256.

Pastick, N. J., Duffy, P., Genet, H., Rupp, T. S., Wylie, B. K., Johnson, K. D., Jorgenson, M. T., Bliss, N., McGuire, A. D., Jafarov, E. E., & Knight, J. F. (2017). Historical and projected trends in landscape drivers affecting carbon dynamics in Alaska. *Ecological Applications,* 27(5), 1383–1402.

Pastick, N. J., Jorgenson, M. T., Wylie, B. K., Nield, S. J., Johnson, K. D., & Finley, A. O. (2015). Distribution of near-surface permafrost in Alaska: Estimates of present and future conditions. *Remote Sensing of Environment,* 168, 301–315.

Perrone, M., Di Febbraro, M., Conti, L., Divíšek, J., Chytrý, M., Keil, P., Carranza, M. L., Rocchini, D., Torresani, M., Moudrý, V., Šímová, P., Prajzlerová, D., Müllerová, J., Wild, J., & Malavasi, M. (2023). The relationship between spectral and plant diversity: Disentangling the influence of metrics and habitat types at the landscape scale. *Remote Sensing of Environment, 293*, 113591.

Queally, N., Ye, Z., Zheng, T., Chlus, A., Schneider, F., Pavlick, R., & Townsend, P. A. (2021). *FlexBRDF: A Flexible BRDF Correction for Grouped Processing of Airborne Imaging Spectroscopy Flightlines* [Preprint]. Biological Sciences.

Rearden, A., Fienup-Riordan, A., Calista Elders Council, & Alaska Native Language Center (Eds.). (2014). *Nunamta elamta-llu Ayuqucia: What our Land and World are Like.* Calista Elders Council and Alaska Native Language Center.

Rocchini, D., Balkenhol, N., Carter, G. A., Foody, G. M., Gillespie, T. W., He, K. S., Kark, S., Levin, N., Lucas, K., Luoto, M., Nagendra, H., Oldeland, J., Ricotta, C., Southworth, J., & Neteler, M. (2010). Remotely sensed spectral heterogeneity as a proxy of species diversity: Recent advances and open challenges. *Ecological Informatics, 5*(5), 318–329.

Rocha, A. V., Loranty, M. M., Higuera, P. E., Mack, M. C., Hu, F. S., Jones, B. M., Breen, A. L., Rastetter, E. B., Goetz, S. J., & Shaver, G. R. (2012). The footprint of Alaskan tundra fires during the past half-century: Implications for surface properties and radiative forcing. *Environmental Research Letters,* 7(4), 044039.

Rossi, C., & Gholizadeh, H. (2023). Uncovering the hidden: Leveraging sub-pixel spectral diversity to estimate plant diversity from space. *Remote Sensing of Environment, 296*, 113734.

Rossi, C., Kneubühler, M., Schütz, M., Schaepman, M. E., Haller, R. M., & Risch, A. C. (2021). Remote sensing of spectral diversity: A new methodological approach to account for spatio-temporal dissimilarities between plant communities. *Ecological Indicators*, 130, 108106.

Sae-Lim, J., Russell, J. M., Vachula, R. S., Holmes, R. M., Mann, P. J., Schade, J. D., & Natali, S. M. (2019). Temperature-controlled tundra fire severity and frequency during the last millennium in the Yukon-Kuskokwim Delta, Alaska. The Holocene, 29(7), 1223–1233.

Savitzky, Abraham., & Golay, M. J. E. (1964). Smoothing and Differentiation of Data by Simplified Least Squares Procedures. *Analytical Chemistry*, 36(8), 1627–1639.

Scenarios Network for Alaska + Arctic Planning (SNAP). (2022). Historical Monthly and Derived Temperature Products Downscaled from CRU TS data via the delta method - 2 km. Retrieved October 17, 2023. (https://catalog.snap.uaf.edu/geonetwork/srv/eng/catalog.search#/metadata/3b2b24ff-4916-4d92-95b7-c6b2fcefd381).

Schmidtlein, S., & Fassnacht, F. E. (2017). The spectral variability hypothesis does not hold across landscapes. *Remote Sensing of Environment*, *192*, 114–125.

Schweiger, A. K., Cavender-Bares, J., Townsend, P. A., Hobbie, S. E., Madritch, M. D., Wang, R., Tilman, D., & Gamon, J. A. (2018). Plant spectral diversity integrates functional and phylogenetic components of biodiversity and predicts ecosystem function. *Nature Ecology & Evolution*, *2*(6), 976–982.

Singh, P., Srivastava, P. K., Malhi, R. K. M., Chaudhary, S. K., Verrelst, J., Bhattacharya, B. K., & Raghubanshi, A. S. (2021). Denoising AVIRIS-NG Data for Generation of New Chlorophyll Indices. *IEEE Sensors Journal*, *21*(5), 6982–6989.

Van Cleemput, E., Adler, P., & Suding, K. N. (2023). Making remote sense of biodiversity: What grassland characteristics make spectral diversity a good proxy for taxonomic diversity? *Global Ecology and Biogeography*, geb.13759.

Wang, R., & Gamon, J. A. (2019). Remote sensing of terrestrial plant biodiversity. *Remote Sensing of Environment*, 231, 111218.

Whittaker, R. H. (1972). Evolution and measurement of species diversity. *Taxon*, 21(2–3), 213–251.